

Effect of Abdominal Wall Inhomogeneities on the Focusing of an Ultrasonic Beam at Different Positions of the Transducer

A. S. Bobina^{a, *}, P. B. Rosnitskiy^a, T. D. Khokhlova^b, P. V. Yuldashev^a, and V. A. Khokhlova^{a, b}

^a Department of Physics, Moscow State University, Moscow, 119991 Russia

^b Division of Gastroenterology, Department of Medicine, University of Washington, Seattle, WA 98195, USA

*e-mail: bobina.as14@physics.msu.ru

Received December 9, 2020; revised January 25, 2021; accepted February 26, 2021

Abstract—A study is performed of the effect acoustic inhomogeneities of the abdominal wall have on the focusing of a powerful ultrasonic beam at different positions of a transducer. A focused beam generated by a 1 MHz transducer is modeled numerically using an acoustic model of the human body created via computer-aided tomography. It is found that the focal maximum of the field of intensity shifts in space, and the maximum achievable intensity in the beam when focusing through the acoustically inhomogeneous abdominal wall is reduced. The best location of the transducer is selected to minimize distortions.

DOI: 10.3103/S1062873821060058

INTRODUCTION

High-intensity focused ultrasound (HIFU) noninvasive surgery has developed rapidly over the last two decades [1]. Therapeutic effects are obtained either through heating the tissue and its thermal denaturation, or by mechanical destruction (histotripsy) of tissue into fragments of subcellular sizes [2–4]. HIFU histotripsy is widely used in different fields of medicine (e.g., treating liver and kidney tumors and eliminating abdominal hematomas) [5, 6].

The general approach to HIFU is to focus an ultrasonic beam at a target area of the body through a coupling medium and tissues in its path. Its advantages are noninvasiveness, no need for a sterile operating room, a reduced risk of infection during surgery, and possible accelerated patient recovery after manipulations [1, 5]. At the same time, a considerable disadvantage of HIFU nowadays is the lack of reliable ways of preliminarily planning surgical intervention for each specific case. An important line of noninvasive ultrasound surgery is therefore developing ways to plan protocols for safe and effective therapeutic intervention.

To solve this problem, we need quantitative data on the parameters of an ultrasonic field in the human body. Such parameters cannot be determined experimentally in a clinical setting. An alternative is to use numerical modeling [7–9]. The problem of a beam passing through the human body is complicated by the difference between the acoustic properties of different biological tissues and organs making the medium of propagation inhomogeneous, which can distort the structure of a focal spot and shift the position of the focus due to refraction [10, 11]. A separate problem is

determining the acoustic properties of different human tissues in one way or another.

In [12], we considered the problem of irradiating the human kidney. We studied the focusing of the ultrasonic beam using an acoustic model based on data obtained via computer-aided tomography. Modeling results showed that the focal maximum is shifted by refraction on tissue inhomogeneities, and its shape is distorted relative to the focal maximum when focusing in a homogeneous medium. At the same time, the effectiveness and accuracy of the therapeutic effect are reduced. We must therefore develop ways of compensating for or reducing distortions due to the inhomogeneity of a medium.

In this work, we studied the effect abdominal wall inhomogeneities have on the focusing of ultrasound at different positions and orientations of the transducer relative to the human body [13, 14]. The problem was considered through the example of using HIFU irradiation to eliminate abdominal hematomas (Fig. 1). In a clinical setting, treatment is based on a powerful ultrasonic beam focused onto a certain area of the hematoma behind the abdominal wall (Fig. 1). The hematoma liquefies under the effect of the ultrasound beam in the histotripsy mode. A thin needle is inserted into the area of irradiation to remove the products of destruction and they are aspirated [6]. Let us consider a case where a hematoma is behind an abdominal wall not far (5–6 cm) from the surface of the skin. At the first stage of our study, the problem is solved in a linear approximation.

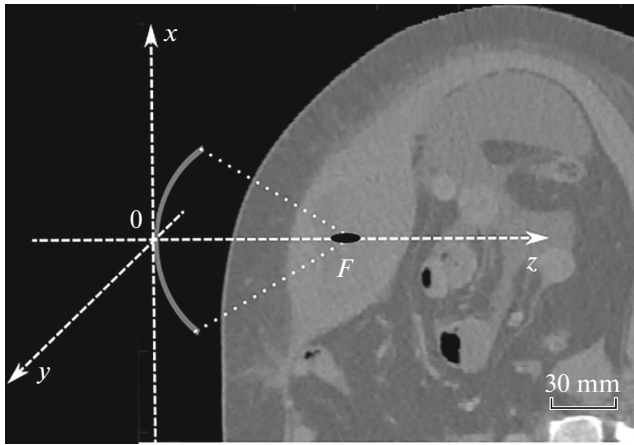


Fig. 1. Geometric pattern of focusing an ultrasonic beam in a human body on a hematoma in the abdominal wall.

ACOUSTIC MODEL OF THE HUMAN BODY

An important step in this work is creating and preparing a realistic model of an acoustically inhomogeneous human body with a hematoma, since we must know all acoustic parameters of the tissue as functions of coordinates in order to construct a numerical solution to the corresponding model equations in a certain domain. For a linear model of wave propagation, these parameters are the speed of sound, density, and coefficient of absorption. The biological medium is inhomogeneous with respect to these characteristics. The speed of sound and density within soft tissues are associated with the relative proportions of water, protein (collagen and hemoglobin), and lipids, and are therefore inherently inhomogeneous [10, 11, 14]. The high content of protein in tissue raises the speed of sound and density, compared to the same parameters in water or blood, while a high content of lipids (e.g., fat) lowers the speed of sound and density.

In this work, the spatial distributions of acoustic parameters were determined using data obtained via computer-aided tomography of the human body. Computer-aided tomography (CT) is one of the most successful nondestructive ways of examining the internal structure of the human body layer by layer. It is based on measuring and using computers to consider the difference between the attenuation of X-ray radiation by tissues of different densities and compositions [15]. The density of tissues at each point of the patient's body can be determined from CT images, the brightness of which is described by the Hounsfield scale [15].

Analysis of the density and speed of sound of different tissues showed that these two parameters strongly correlate with each other, and a linear relationship can be established between them [16]. Using the established ratios, we can reconstruct the speed-of-sound distribution at each point of the acoustic model. On the other hand, it was found that the coefficient of

absorption correlates poorly with the density, so this parameter must be restored another way. The acoustic model was therefore segmented (i.e., different types of tissues and organs were selected and numbered). Different tissues (skin, fat, muscle, hematoma, and bone) were selected from CT images based on speed-of-sound thresholds [12]. When constructing three-dimensional matrices of acoustic parameters, the segmented regions were assigned values of the coefficient of absorption known from the literature [17]. Subsequent work was done only with segmented data and two matrices containing the distributions of the speed of sound and density in a medium.

Data of the acoustic model of an inhomogeneous medium were obtained with discretization intervals of CT images in a Cartesian coordinate system in directions x and y with steps of $\Delta x = \Delta y = 0.77$ mm (across the human body) and in direction z with a step of $\Delta z = 2.5$ mm (along the human body). This step of the matrix of inhomogeneities is quite large and comparable to the size of the focal region of the ultrasonic beam, so analyzing the change in focus shape, the formation of side maxima, and other important characteristics becomes impossible if such a matrix is used directly in acoustic modeling. To ensure the accuracy of calculations for the acoustic field, we therefore reduced the intervals of discretization to values of $\Delta x = \Delta y = \Delta z = 0.5$ mm using the trilinear interpolation in the MATLAB software. The distributions of the acoustic parameters of the medium were then transferred to a numerical grid in the Cartesian coordinate system associated with the transducer, where axis z is directed along that of the ultrasonic beam (Fig. 1).

When determining the best direction of radiation, it is important to avoid the ultrasonic beam hitting the patient's bones and organs that contain air. Bones strongly absorb and reflect ultrasound, which can result in overheating and burns. Air bubbles in the path of the ultrasonic beam cause it to reflect and scatter. Positioning the transducer so that the beam it creates passes the shortest path through soft tissues to the focal point would seem to be the best solution, since it reduces the effects of absorption in the tissue and the effects of refraction shifting the focus. In this work, a hematoma behind the human abdominal wall is considered an object of the HIFU therapeutic effect. This is an easy object to irradiate, since it is close to the skin, far from the ribs and pelvic bones, and far from the air cavities formed in the intestinal tract and other gas-containing organs. The main parameter for choosing the optimum location of the transducer is the angle at which the ultrasonic beam penetrates into soft tissues almost perpendicular to the skin surface.

After selecting the area and direction of irradiation, the 3D matrix of acoustic parameters obtained from the CT image was rotated so that axis z of the new coordinate system coincided with that of the ultrasonic beam. In mathematical modeling, the human body rotates about the main axis of the transducer, and the transducer does not rotate about the model. To

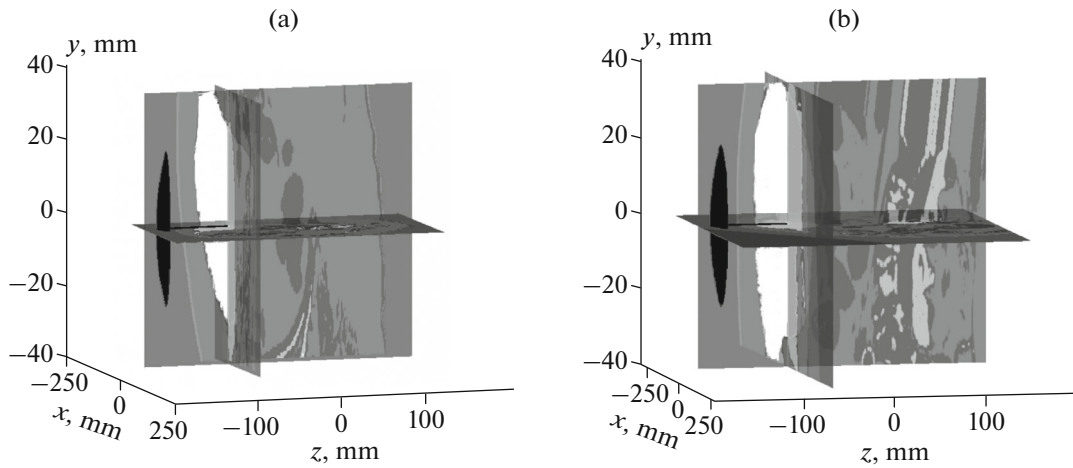


Fig. 2. Results from rotating the segmented 3D matrix with abdominal wall hematoma. (a) Position 1 before rotation; (b) position 2 after rotation. The hematoma is shown in white; the transducer is shown in black. Water and other organs are shown in different shades of gray.

accomplish this, we must transfer the 3D matrices containing information on the speed of sound, density, and coefficient of absorption in each $0.5 \times 0.5 \times 0.5$ mm volume of the irradiation medium in the coordinate system to a new coordinate system. A rotation matrix is normally used to perform a direct orthogonal transformation in Euclidean space. It contains information about the angle of rotation and the axis around which rotation is performed. Any rotation in three-dimensional space can thus be presented as a composition of rotations around three orthogonal axes. The composition is the matrix resulting from the product of the corresponding three rotation matrices for each axis. For convenience, the rotation matrix is expressed in terms of Euler angles describing the rotation of an absolutely rigid body in three-dimensional Euclidean space. These are angles that correspond to rotation around one axis, and rotations around all axes are performed in sequence. Rotation is first done around axis Oz by angle α of precession. Rotation is then done around new axis Ox' (formed after the first rotation) by angle β of nutation, and the last rotation is done around the newest axis Oz' (formed after the first and the second rotations) by angle γ of proper rotation. A rotation matrix is written for each step:

$$\begin{aligned}
 R_z(-\alpha) &= \begin{pmatrix} \cos(\alpha) & \sin(\alpha) & 0 \\ -\sin(\alpha) & \cos(\alpha) & 0 \\ 0 & 0 & 1 \end{pmatrix}; \\
 R_x(-\beta) &= \begin{pmatrix} 1 & 0 & 0 \\ 0 & \cos(\beta) & \sin(\beta) \\ 0 & -\sin(\beta) & \cos(\beta) \end{pmatrix}, \\
 R_z(-\gamma) &= \begin{pmatrix} \cos(\gamma) & \sin(\gamma) & 0 \\ -\sin(\gamma) & \cos(\gamma) & 0 \\ 0 & 0 & 1 \end{pmatrix}.
 \end{aligned} \tag{1}$$

The final rotation matrix can be obtained by multiplying these three matrices:

$$R = R_z(-\alpha)R_x(-\beta)R_z(-\gamma). \tag{2}$$

Resulting matrix (2) was used to recalculate the coordinates from the existing system to the one selected system as the best. The choice of the angle was based on using one of several locations where the maximum perpendicularity of the beam to the skin was likely to be observed. The final result is shown in Fig. 2, where Fig. 2a corresponds to the position of the transducer before rotation, and Fig. 2b corresponds to the position of the transducer after rotation. The hematoma is shown in white, and the transducer is shown in black. All other types of biological tissues and the coupling medium (water) are shown in different shades of gray.

THEORETICAL MODEL AND FOCUSING PARAMETERS

The propagation of an ultrasonic beam with frequency $f_0 = 1$ MHz in an inhomogeneous biological tissue was modeled using the freely available k-Wave toolkit for the MathLab software designed to describe acoustic wave fields [18]. Numerical k-Wave procedures allow us to model acoustic waves in inhomogeneous media with a power law of absorption [19]. To calculate the field of a high-intensity ultrasonic wave in the human body, the governing equations normally must consider the combined effects of diffraction, nonlinearity, absorption, dispersion, and inhomogeneity of the acoustic medium (i.e., the difference between such acoustic parameters of tissues and organs as the speed of sound, density, absorption, and nonlinearity). The corresponding equations can be written as a system of differential equations in partial

Table 1. Values of the acoustic parameters of soft tissues in the model [16]

Tissue	c_0 , m s ⁻¹	ρ_0 , kg m ⁻³	α , dB m ⁻¹
Water	1500	1000	0
Skin	1580–1630	1090	182.4
Fat	1450–1480	950	38.2
Bone	≥2000	≥1800	1311.6
Hematoma (blood clot)	1580–1630	1060	26.05
Muscle	1550–1580	1050	104.23

derivatives of the first order. In this work, we used the linearized form of the equations:

$$\begin{aligned} \frac{\partial \vec{u}}{\partial t} &= -\frac{1}{\rho_0} \nabla p, \quad \frac{\partial p}{\partial t} = -\rho_0 \nabla \vec{u} - \vec{u} \nabla \rho_0, \\ p &= c_0^2 \left(\rho + \vec{d} \nabla \rho_0 - \frac{\delta}{c_0^2} \frac{\partial p}{\partial t} \right). \end{aligned} \quad (3)$$

Here, \vec{u} is the vector of a particle's velocity in the medium; \vec{d} is the vector of displacement of particles of the medium; p is the acoustic pressure; ρ denotes fluctuations in density; $\rho_0(\vec{r})$, $c_0(\vec{r})$, and $\delta(\vec{r})$ are the equilibrium density, the speed of sound, and the dissipative coefficient of the inhomogeneous medium, respectively; and \vec{r} is the radius vector. Dissipative coefficient δ is assumed to be zero in water. For the segments of the inhomogeneous abdominal wall, we use an unambiguous relationship $\delta = 2\alpha c_0 / (2\pi f_0)$ between the dissipative coefficient δ and the absorption coefficient α at the frequency of $f_0 = 1$ MHz from the literature [17]. The values of the absorption coefficients, the ranges of the speed of sound and density of various soft tissues used in the model of the human body are presented in Table 1.

System (3) was solved using the pseudospectral method, where the spatial gradients of the acoustic field are calculated in k -space based on the Fourier transform, and the two-layer time integration scheme includes a correction to compensate for the numerical dispersion. In the simulation, a transducer with an operating frequency of 1 MHz, a focal length of 85 mm, a central hole diameter of 30 mm, and an aperture of 85 mm is considered. The boundary condition in the form of the initial particle velocity on the $z = 0$ plane was calculated using the Rayleigh integral for a grid step of 0.5 mm under the assumption that the amplitude of the normal component of the particle velocity of the transducer surface is uniform. The beam was focused into the hematoma area to a depth of 64 mm in the position before rotation (Fig. 2a) and 55 mm in the position after rotation (Fig. 2b). By changing the direction of wave propagation through the water-and-skin interface, it was possible to determine the optimal location of the transducer, at which the acoustic pressure field in amplitude and shape

would be closest to the amplitude and shape of the field when focusing in a homogeneous medium (water). The calculations were carried out in the coordinate system bound with the transducer. The spatial distributions of acoustic parameters were rotated at specified angles around the point of the geometric focus of the transducer (Fig. 2), after which the parameters of the medium at the nodes of the numerical grid bound with the transducer were determined. The results of calculating the acoustic field for each angle were compared with each other.

RESULTS AND DISCUSSION

Our modeling results are presented in Fig. 3, which shows the spatial distributions of the intensity normalized to the intensity at the transducer along the z (Fig. 3a), x (Fig. 3b), and y (Fig. 3c) axes, and in Fig. 4, which shows the spatial distributions of the field pressure amplitude normalized to the pressure at the transducer, in the axial planes of the transducer xz and yz , and in the focal plane xy for the cases of different positions of the transducer relative to the body, as well as in a homogeneous medium (water). To check the correctness and accuracy of numerical calculations, an analytical solution on the beam axis obtained using the Rayleigh integral in water is also shown (Fig. 3). This graph almost completely coincides with the graph of the solution for the intensity field in water obtained by the k-Wave method, which shows the correctness of the program and allows it to be used for more complex cases, the analytical solution of which cannot be calculated.

Figures 4a–4c show the spatial distributions of the field pressure amplitude normalized to the pressure at the transducer in a homogeneous medium without absorption (water), which are considered reference in this work. When the transducer is positioned as in Fig. 2a (before rotation), the acoustic field in the hematoma is shown in Figs. 4d–4f. The acoustic field in the hematoma is shown in Figs. 4g–4i for when the transducer is positioned as in Fig. 2b (after rotation). We can see that the focal maximum is distorted when there are inhomogeneities. It changes its shape and shifts from its initial position on the transducer axis (Figs. 4d–4f and 4g–4i) relative to the case of water

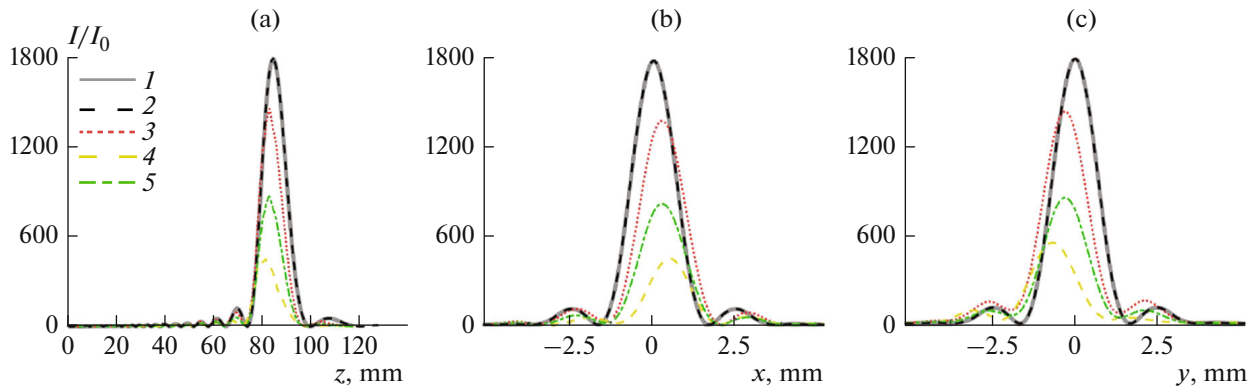


Fig. 3. Results from linear modeling of a beam focusing in water and inhomogeneous tissue. Intensity distributions normalized to the intensity at the transducer (a) along the z axis of the beam, and in the focal plane in the (b) x and (c) y directions, respectively. The curves correspond to options for calculating the field (I) in water (a pseudospectral k-Wave model), (2) in water (a Rayleigh integral model), (3) in an inhomogeneous medium before rotation of the CT matrix and ignoring absorption (a k-Wave model), (4) in an inhomogeneous medium before rotation of the CT matrix and ignoring absorption (a W-wave model), and (5) in an inhomogeneous medium after rotation of the CT matrix and ignoring absorption (a k-Wave model).

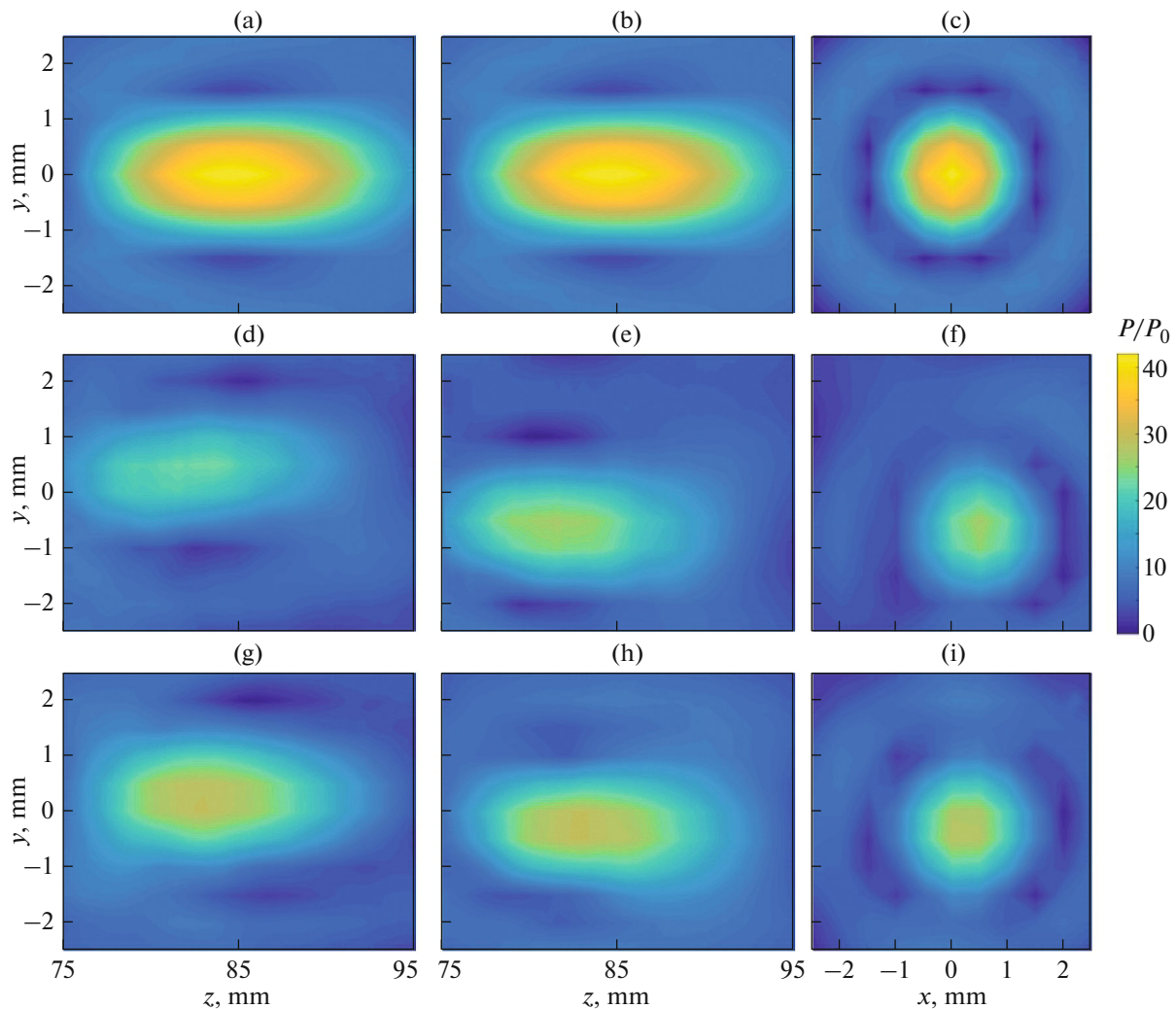


Fig. 4. Results from linear modeling of the transducer field in (a, b, c) water and (d, e, f) inhomogeneous absorbing tissue before rotation and (g, h, i) after rotation. The distributions of the pressure amplitude normalized to the pressure amplitude at the transducer are plotted in axial planes (a, d, g) yz and (b, e, h) xz , and in focal plane (c, f, i) xy .

(Figs. 4a–4c). When the irradiation is oblique to the surface of the skin (Fig. 2a), the focal spot is distorted due to the refraction of rays at the boundaries of tissue layers and is shifted from the beam axis in directions x and y by 0.5 mm (Figs. 3b, 3c). It is also shifted 3.5 mm closer to the transducer along axis z (Fig. 3a). In addition, the refraction at tissue inhomogeneities and absorption reduces the amplitude of pressure at the focus, which complicates obtaining the therapeutic effect of ultrasound on the tissue. When the beam axis is perpendicular to the tangent to the skin surface (Fig. 2b), the focal spot retains its shape and shifts 2 mm closer to the transducer along axis z (Fig. 3a). The shift along axis y is about 0.5 mm, while the focus remains stationary along axis x (Figs. 3b, 3c).

When focusing at an angle, the intensity of the focus falls by 83% (Fig. 2a) relative to focusing in water. When focusing perpendicular to the surface of the skin (the transducer is positioned as in Fig. 2b), the intensity of the focus falls by 51%, which can be seen in the graphs in Fig. 3. After a better position was selected, the intensity of the focus grew by more than 30%, compared to the one at the position before the rotation.

We estimated the contribution from absorption to the total loss of intensity at the focus. To do so, we modeled focusing in an inhomogeneous medium with zero absorption when the transducer was in the position before rotation (Fig. 3). It was shown that the contribution to absorption losses was 63% of all intensity losses at the focus. However, the contributions from absorption and refraction to losses could change in other cases of abdominal wall inhomogeneity, or at a deeper locations of the focus. We plan to study more complex cases of the location of hematoma in the human body. However, the importance and effectiveness of preliminarily planning surgery with the optimum choice of radiation was already confirmed by a case that can be considered simple.

CONCLUSIONS

A theoretical model for describing the focusing of ultrasonic beams in inhomogeneous soft tissues of the human body was built by numerically solving equations of linear acoustics in an inhomogeneous medium with frequency-dependent absorption using the k-Wave package. We modeled the ultrasonic beam generated by a therapeutic transducer focused on an abdominal hematoma at a depth of 55 and 64 mm at different positions of the transducer. It was shown that the drop in intensity at the focal point can be around 80% due to tissue absorption and the effect of beam aberrations in an inhomogeneous medium, compared to focusing in water. Absorption, which can be compensated for by raising the power of the transducer, is approximately half these losses. The refraction of the beam on the surface of the body and inhomogeneities in the speed of sound during wave propagation shifts

the focal point in the longitudinal and transverse directions by distances of up to 1 mm and distorts the shape of the focal spot. The influence of these effects depends on the location of the transducer, which must be considered when developing ultrasonic irradiation protocols.

FUNDING

This work was supported by the Russian Foundation for Basic Research, project no. 20-02-00210a.

REFERENCES

1. Gavrilov, L.R., *Fokusirovannyi ul'trazvuk vysokoi intensivnosti v meditsine* (High-Intensity Focused Ultrasound in Medicine), Moscow: Fазis, 2013.
2. Bailey, M.R., Khokhlova, V.A., Sapozhnikov, O.A., et al., *Acoust. Phys.*, 2003, vol. 49, no. 4, p. 369.
3. Maxwell, A., Sapozhnikov, O., Bailey, M., et al., *Acoust. Today*, 2012, vol. 8, no. 4, p. 24.
4. Khokhlova, V.A., Fowlkes, J.B., Roberts, W.W., et al., *Int. J. Hyperthermia*, 2015, vol. 31, no. 2, p. 145.
5. Dubinsky, T.J., Cuevas, C., Dighe, M.K., et al., *Am. J. Roentgenol.*, 2008, vol. 190, p. 191.
6. Khokhlova, T.D., Monsky, W.L., Haider, Y.A., et al., *Ultrasound Med. Biol.*, 2016, vol. 42, no. 7, p. 1491.
7. Gu, J. and Jing, Y., *IEEE Trans. Ultrason., Ferroelectr., Freq. Control*, 2015, vol. 62, no. 11, p. 1979.
8. Jing, Y. and Cleveland, R.O., *J. Acoust. Soc. Am.*, 2007, vol. 122, p. 1352.
9. Shvetsov, I.A., Shcherbinin, S.A., Astafiev, P.A., et al., *Bull. Russ. Acad. Sci.: Phys.*, 2018, vol. 82, no. 3, p. 355.
10. Taraldsen, G., *IEEE Trans. Ultrason., Ferroelectr., Freq. Control*, 2005, vol. 52, no. 9, p. 1473.
11. Sukhoruchkin, D.A., Yuldashev, P.V., Tsysar, S.A., et al., *Bull. Russ. Acad. Sci.: Phys.*, 2018, vol. 82, no. 3, p. 507.
12. Bobina, A.S., Khokhlova, V.A., and Yuldashev, P.V., in *Sb. tr. XVI Vseross. shkoly-seminara "Fizika i primeneniye mikrovoln"* (Proc. XVI All-Russian School-Seminar "Physics and Application of Microwaves"), Moscow, 2017, p. 7.
13. Mast, T.D., Hinkelman, L.M., Orr, M.J., et al., *J. Acoust. Soc. Am.*, 1997, vol. 102, p. 1177.
14. Treeby, B.E. and Cox, B.T., *J. Biomed. Opt.*, 2010, vol. 15, no. 2, 021314.
15. Schneideryx, U. and Pedroni, E., *Phys. Med. Biol.*, 1996, vol. 41, p. 111.
16. Mast, T.D., *Acoust. Res. Lett. Online*, 2000, vol. 1, no. 2, p. 37.
17. Duck, F.A., *Physical Properties of Tissue: A Comprehensive Reference Book*, London: Academic, 1990.
18. k-Wave. <http://www.k-wave.org>.
19. Jaros, J., Rendell, A.P., and Treeby, B.E., *Int. J. High Perform., C*, 2016, vol. 30, no. 2, p. 137.

Translated by I. Obrezanova